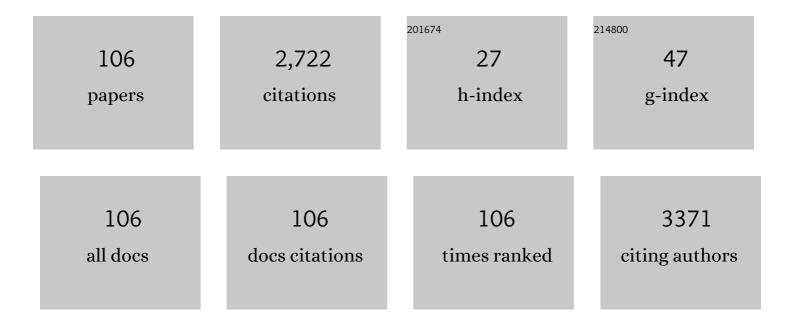
List of Publications by Year in descending order

Source: https://exaly.com/author-pdf/8855425/publications.pdf Version: 2024-02-01



SAM LIN CHOL

#	Article	IF	CITATIONS
1	An excitation wavelength-optimized, stable SERS biosensing nanoplatform for analyzing adenoviral and AstraZeneca COVID-19 vaccination efficacy status using tear samples of vaccinated individuals. Biosensors and Bioelectronics, 2022, 204, 114079.	10.1	11
2	Biological SERS-active sensor platform based on flexible silk fibroin film and gold nanoislands. Optics Express, 2022, 30, 7782.	3.4	4
3	Effect of Dentin Desensitizer Containing Novel Bioactive Glass on the Permeability of Dentin. Materials, 2022, 15, 4041.	2.9	1
4	Adiponectin-targeted SERS immunoassay biosensing platform for early detection of gestational diabetes mellitus. Biosensors and Bioelectronics, 2022, 213, 114488.	10.1	12
5	Wavelength-dependent label-free identification of isolated nontuberculous mycobacteria using surface-enhanced Raman spectroscopy. Spectrochimica Acta - Part A: Molecular and Biomolecular Spectroscopy, 2021, 248, 119186.	3.9	5
6	Label-free breast cancer detection using fiber probe-based Raman spectrochemical biomarker-dominated profiles extracted from a mixture analysis algorithm. Analytical Methods, 2021, 13, 3249-3255.	2.7	6
7	A facile, portable surface-enhanced Raman spectroscopy sensing platform for on-site chemometrics of toxic chemicals. Sensors and Actuators B: Chemical, 2021, 343, 130102.	7.8	19
8	Effect of Novel Bioactive Glass-Containing Dentin Adhesive on the Permeability of Demineralized Dentin. Materials, 2021, 14, 5423.	2.9	4
9	Label-Free Surface-Enhanced Raman Spectroscopy Biosensor for On-Site Breast Cancer Detection Using Human Tears. ACS Applied Materials & Interfaces, 2020, 12, 7897-7904.	8.0	83
10	Surface analysis of metal clips of ceramic self-ligating brackets. Korean Journal of Orthodontics, 2019, 49, 12.	2.3	2
11	Effects of scleral collagen crosslinking with different carbohydrate on chemical bond and ultrastructure of rabbit sclera: Future treatment for myopia progression. PLoS ONE, 2019, 14, e0216425.	2.5	8
12	A recyclable CNC-milled microfluidic platform for colorimetric assays and label-free aged-related macular degeneration detection. Sensors and Actuators B: Chemical, 2019, 290, 484-492.	7.8	10
13	A rapid tag-free identification of <i>Escherichia coli</i> antibiotic-resistant isolates using Raman scattering. Analytical Methods, 2019, 11, 5381-5387.	2.7	8
14	A label-free cellulose SERS biosensor chip with improvement of nanoparticle-enhanced LSPR effects for early diagnosis of subarachnoid hemorrhage-induced complications. Biosensors and Bioelectronics, 2018, 111, 59-65.	10.1	59
15	Labelâ€free monitoring of inflammatory tissue conditions using a carrageenanâ€induced acute inflammation rat model. Microscopy Research and Technique, 2018, 81, 544-550.	2.2	1
16	Poly(lactide-co-glycolide) nanofibrous scaffolds chemically coated with gold-nanoparticles as osteoinductive agents for osteogenesis. Applied Surface Science, 2018, 432, 300-307.	6.1	35
17	A simple and facile paper-based colorimetric assay for detection of free hydrogen sulfide in prostate cancer cells. Sensors and Actuators B: Chemical, 2018, 256, 828-834.	7.8	41
18	A Fully Integrated Paper-Microfluidic Electrochemical Device for Simultaneous Analysis of Physiologic Blood Ions. Sensors, 2018, 18, 104.	3.8	23

#	Article	IF	CITATIONS
19	Paper-Based Surface-Enhanced Raman Spectroscopy for Diagnosing Prenatal Diseases in Women. ACS Nano, 2018, 12, 7100-7108.	14.6	101
20	Highly Reproducible Au-Decorated ZnO Nanorod Array on a Graphite Sensor for Classification of Human Aqueous Humors. ACS Applied Materials & Interfaces, 2017, 9, 5891-5899.	8.0	52
21	Rapid label-free identification of Klebsiella pneumoniae antibiotic resistant strains by the drop-coating deposition surface-enhanced Raman scattering method. Spectrochimica Acta - Part A: Molecular and Biomolecular Spectroscopy, 2017, 183, 53-59.	3.9	36
22	Fabrication of a SERS-encoded microfluidic paper-based analytical chip for the point-of-assay of wastewater. International Journal of Precision Engineering and Manufacturing - Green Technology, 2017, 4, 221-226.	4.9	23
23	Low-Cost Label-Free Biosensing Bimetallic Cellulose Strip with SILAR-Synthesized Silver Core–Gold Shell Nanoparticle Structures. Analytical Chemistry, 2017, 89, 6448-6454.	6.5	51
24	Controlling successive ionic layer absorption and reaction cycles to optimize silver nanoparticle-induced localized surface plasmon resonance effects on the paper strip. Spectrochimica Acta - Part A: Molecular and Biomolecular Spectroscopy, 2017, 174, 37-43.	3.9	12
25	Label-free identification of antibiotic resistant isolates of living <i>Escherichia coli</i> : Pilot study. Microscopy Research and Technique, 2017, 80, 177-182.	2.2	16
26	Microfluidicâ€based nonâ€enzymatic glycation enhances crossâ€linking of human scleral tissue compared to conventional soaking. Scanning, 2016, 38, 421-426.	1.5	4
27	A solvent-free microbial-activated air cathode battery paper platform made with pencil-traced graphite electrodes. Scientific Reports, 2016, 6, 28588.	3.3	30
28	A stand-alone pressure-driven 3D microfluidic chemical sensing analytic device. Sensors and Actuators B: Chemical, 2016, 230, 380-387.	7.8	20
29	Instrument-Free Synthesizable Fabrication of Label-Free Optical Biosensing Paper Strips for the Early Detection of Infectious Keratoconjunctivitides. Analytical Chemistry, 2016, 88, 5531-5537.	6.5	48
30	Label-free optical detection of age-related and diabetic oxidative damage in human aqueous humors. Microscopy Research and Technique, 2016, 79, 1050-1055.	2.2	7
31	Biochemical fingerprints of human papillomavirus infection and cervical dysplasia using cervical fluids: Spectral pattern investigation. Microscopy Research and Technique, 2016, 79, 966-972.	2.2	8
32	Morphological investigation of various orthodontic lingual bracket slots using scanning electron microscopy and atomic force microscopy. Microscopy Research and Technique, 2016, 79, 1193-1199.	2.2	5
33	A low-cost, monometallic, surface-enhanced Raman scattering-functionalized paper platform for spot-on bioassays. Sensors and Actuators B: Chemical, 2016, 222, 1112-1118.	7.8	67
34	Biochemical investigations of human papillomavirusâ€infected cervical fluids. Microscopy Research and Technique, 2015, 78, 200-206.	2.2	20
35	Correlation between frictional force and surface roughness of orthodontic archwires. Scanning, 2015, 37, 399-405.	1.5	20
36	ln vitro slidingâ€driven morphological changes in representative esthetic <scp>NiTi</scp> archwire surfaces. Microscopy Research and Technique, 2015, 78, 926-934.	2.2	9

#	Article	IF	CITATIONS
37	Surface ultrastructure and mechanical properties of three different white oated NiTi archwires. Scanning, 2015, 37, 414-421.	1.5	25
38	Enhanced biocompatibility and wound healing properties of biodegradable polymer-modified allyl 2-cyanoacrylate tissue adhesive. Materials Science and Engineering C, 2015, 51, 43-50.	7.3	27
39	Facile Fabrication of a Silver Nanoparticle Immersed, Surface-Enhanced Raman Scattering Imposed Paper Platform through Successive Ionic Layer Absorption and Reaction for On-Site Bioassays. ACS Applied Materials & Interfaces, 2015, 7, 27910-27917.	8.0	82
40	A low-cost ion detecting device with paper-based disposal sensor. , 2015, , .		0
41	Paper-based printed circuit boards. , 2015, , .		2
42	A novel cardiac spectral envelope extraction algorithm using a single-degree-of-freedom vibration model. Biomedical Signal Processing and Control, 2015, 18, 169-173.	5.7	4
43	Effects of aging procedures on the molecular, biochemical, morphological, and mechanical properties of vacuum-formed retainers. Journal of the Mechanical Behavior of Biomedical Materials, 2015, 51, 356-366.	3.1	33
44	Paper-based 3D microfluidic device for multiple bioassays. Sensors and Actuators B: Chemical, 2015, 219, 245-250.	7.8	62
45	Investigation of nanostructural changes following acute injury using atomic force microscopy in rabbit vocal folds. Microscopy Research and Technique, 2015, 78, 569-576.	2.2	9
46	Evaluation of aneurysm-associated wall shear stress related to morphological variations of circle of Willis using a microfluidic device. Journal of Biomechanics, 2015, 48, 348-353.	2.1	26
47	GS1-26 INITIAL FORCE DELIVERY CHARACTERISTICS OF LIGATION ON NANOSTUCTURE AND MECHANICAL PROPERTIES OF NITI SHAPE MEMORY ALLOYS(GS1: Cell and Tissue Biomechanics). The Proceedings of the Asian Pacific Conference on Biomechanics Emerging Science and Technology in Biomechanics, 2015, 2015.8, 137.	0.0	0
48	Medical Applications of Atomic Force Microscopy and Raman Spectroscopy. Journal of Nanoscience and Nanotechnology, 2014, 14, 71-97.	0.9	33
49	Evaluation of antibiotic effects on Pseudomonas aeruginosa biofilm using Raman spectroscopy and multivariate analysis. Biomedical Optics Express, 2014, 5, 3238.	2.9	70
50	Inflammatory responses and morphological changes of radiofrequencyâ€induced rat sciatic nerve fibres. European Journal of Pain, 2014, 18, 192-203.	2.8	19
51	Label-Free Biochemical Analytic Method for the Early Detection of Adenoviral Conjunctivitis Using Human Tear Biofluids. Analytical Chemistry, 2014, 86, 11093-11099.	6.5	47
52	Analysis of cerebral blood flow by pneumatic-valves-controlled microfluidic device: risk assessment of infarction correlated with morphometric variation of cerebral vascular system. Microfluidics and Nanofluidics, 2014, 17, 843-853.	2.2	1
53	A novel cardiac spectral segmentation based on a multi-Gaussian fitting method for regurgitation murmur identification. Signal Processing, 2014, 104, 339-345.	3.7	13
54	Molecular and chemical investigations and comparisons of biomaterials for ocular surface regeneration. Microscopy Research and Technique, 2014, 77, 183-188.	2.2	12

#	Article	IF	CITATIONS
55	Clinicoâ€biochemical investigations of aging effects on normoglycemic and hyperglycemic murine retinal tissues. Microscopy Research and Technique, 2014, 77, 1023-1030.	2.2	6
56	Short-Term Response of Mitomycin C on the Human Rectus Muscle Following Strabismus Surgery: Histological, Ultrastructural, and Biomechanical Evaluation. Microscopy and Microanalysis, 2013, 19, 227-232.	0.4	6
57	Short-term effect of cryotherapy on human scleral tissue by atomic force microscopy. Scanning, 2013, 35, 302-307.	1.5	11
58	Structural response of human corneal and scleral tissues to collagen cross-linking treatment with riboflavin and ultraviolet A light. Lasers in Medical Science, 2013, 28, 1289-1296.	2.1	40
59	Postoperative effect of radiofrequency treatments on the rabbit dermal collagen fibrillary matrix. Microscopy Research and Technique, 2013, 76, 219-224.	2.2	3
60	Nanostructural and Nanomechanical Responses of Collagen Fibrils in the Collagenase-Induced Achilles Tendinitis Rat Model. Journal of Nanoscience and Nanotechnology, 2013, 13, 7279-7286.	0.9	6
61	Structural and Biomechanical Effects of Photooxidative Collagen Cross-Linking with Photosensitizer Riboflavin and 370 nm UVA Light on Human Corneoscleral Tissues. Microscopy and Microanalysis, 2013, 19, 1334-1340.	0.4	17
62	Nanostructural Response of Mitomycin C Application on Human Scleral Tissues. Journal of Biomedical Nanotechnology, 2013, 9, 1393-1397.	1.1	3
63	Inflammatory Effect of Monopolar Radiofrequency Treatment on Collagen Fibrils in Rabbit Skins. Journal of Biomedical Nanotechnology, 2013, 9, 1403-1407.	1.1	8
64	Internal-Specific Morphological Analysis of Sciatic Nerve Fibers in a Radiofrequency-Induced Animal Neuropathic Pain Model. PLoS ONE, 2013, 8, e73913.	2.5	19
65	Biocompatibility of a Novel Cyanoacrylate Based Tissue Adhesive: Cytotoxicity and Biochemical Property Evaluation. PLoS ONE, 2013, 8, e79761.	2.5	22
66	Scanning Electron Microscopy Study of the Effect of the Brushing Time on the Human Tooth Dentin After Exposure to Acidic Softdrinks. Journal of Nanoscience and Nanotechnology, 2012, 12, 5199-5204.	0.9	2
67	Short-term nanostructural effects of high radiofrequency treatment on the skin tissues of rabbits. Lasers in Medical Science, 2012, 27, 923-933.	2.1	10
68	Effects of extracorporeal shockwave therapy on nanostructural and biomechanical responses in the collagenase-induced Achilles tendinitis animal model. Lasers in Medical Science, 2012, 27, 1195-1204.	2.1	21
69	Real time measurement of myocardial oxygen dynamics during cardiac ischemia–reperfusion of rats. Analyst, The, 2012, 137, 5312.	3.5	10
70	AFM Study for Morphological Characteristics and Biomechanical Properties of Human Cataract Anterior Lens Capsules. Scanning, 2012, 34, 247-256.	1.5	21
71	Effects of selfâ€ligating brackets on the surfaces of stainless steel wires following clinical use: AFM investigation. Journal of Microscopy, 2012, 246, 53-59.	1.8	10
72	Potential effects of toothâ€brushing on human dentin wear following exposure to acidic soft drinks. Journal of Microscopy, 2012, 247, 176-185.	1.8	11

#	Article	IF	CITATIONS
73	Nanostructural effect of acid-etching and fluoride application on human primary and permanent tooth enamels. Materials Science and Engineering C, 2012, 32, 1127-1132.	7.3	2
74	Ultrastructural effect of selfâ€ligating bracket materials on stainless steel and superelastic niTi wire surfaces. Microscopy Research and Technique, 2012, 75, 1076-1083.	2.2	10
75	Effect of extracorporeal shockwave therapy on nanostructural and property responses of the Achilles tendinitis rat model. , 2011, , .		0
76	Development of a joint space width measurement method based on radiographic hand images. Computers in Biology and Medicine, 2011, 41, 987-998.	7.0	10
77	Effects of Mitomycin C on Scleral Collagen Fibrils According to Atomic Force Microscopy. Journal of Korean Ophthalmological Society, 2011, 52, 671.	0.2	0
78	Changes in Collagen Fibril Pattern and Adhesion Force with Collagenase-Induced Injury in Rat Achilles Tendon Observed via AFM. Journal of Nanoscience and Nanotechnology, 2011, 11, 773-777.	0.9	12
79	Investigation of aging effects in human hair using atomic force microscopy. Skin Research and Technology, 2011, 17, 63-68.	1.6	20
80	Neuroprotective effects of magnesium-sulfate on ischemic injury mediated by modulating the release of glutamate and reduced of hyperreperfusion. Brain Research, 2011, 1371, 121-128.	2.2	32
81	Evaluation of inflammatory change and bone erosion using a murine type II collagen-induced arthritis model. Rheumatology International, 2011, 31, 595-603.	3.0	12
82	Non-invasive screening of progressive joint defects in the Type II collagen-induced arthritis animal model using radiographic paw images. Inflammation Research, 2011, 60, 447-456.	4.0	6
83	Changes in Ultrastructure and properties of bracket slots after Orthodontic treatment with bicuspid extraction. Scanning, 2011, 33, 25-32.	1.5	18
84	Nanostructural investigation of frontalis sling biomaterial surfaces. Scanning, 2011, 33, 419-425.	1.5	8
85	Ultrastructural investigation of intact orbital implant surfaces using atomic force microscopy. Scanning, 2011, 33, 211-221.	1.5	18
86	Selection of wavelet packet measures for insufficiency murmur identification. Expert Systems With Applications, 2011, 38, 4264-4271.	7.6	35
87	AFM Study for Morphological and Mechanical Properties of Human Scleral Surface. Journal of Nanoscience and Nanotechnology, 2011, 11, 6382-6388.	0.9	17
88	Effect of cross-linking with riboflavin and ultraviolet A on the chemical bonds and ultrastructure of human sclera. Journal of Biomedical Optics, 2011, 16, 125004.	2.6	26
89	Neuroprotective Effects by Nimodipine Treatment in the Experimental Global Ischemic Rat Model : Real Time Estimation of Glutamate. Journal of Korean Neurosurgical Society, 2011, 49, 1.	1.2	14

90 Wavelet packet based features for insufficient murmur identification. , 2010, , .

3

#	Article	IF	CITATIONS
91	Biomechanical analysis of dynamic behavior in human postural control. , 2010, , .		3
92	Correlation between extracellular glutamate release and neuronal cell death in an eleven vessel occlusion model in rat. Brain Research, 2010, 1342, 160-166.	2.2	7
93	Effects of fluoride treatment on phosphoric acid-etching in primary teeth: An AFM observation. Micron, 2010, 41, 498-506.	2.2	16
94	Cardiac sound murmurs classification with autoregressive spectral analysis and multi-support vector machine technique. Computers in Biology and Medicine, 2010, 40, 8-20.	7.0	113
95	Development of ECG beat segmentation method by combining lowpass filter and irregular R–R interval checkup strategy. Expert Systems With Applications, 2010, 37, 5208-5218.	7.6	46
96	The Role of Clutamate Release on Voltage-Dependent Anion Channels (VDAC)-Mediated Apoptosis in an Eleven Vessel Occlusion Model in Rats. PLoS ONE, 2010, 5, e15192.	2.5	15
97	Real-time ischemic condition monitoring in normoglycemic and hyperglycemic rats. Physiological Measurement, 2010, 31, 439-450.	2.1	6
98	Potential neuroprotective effects of acupuncture stimulation on diabetes mellitus in a global ischemic rat model. Physiological Measurement, 2010, 31, 633-647.	2.1	20
99	Effect of fluoride pretreatment on primary and permanent tooth surfaces by acidâ€etching. Scanning, 2010, 32, 375-382.	1.5	16
100	Detecting Specific Health-Related Events Using an Integrated Sensor System for Vital Sign Monitoring. Sensors, 2009, 9, 6897-6912.	3.8	18
101	Development of QRS detection algorithm designed for wearable cardiorespiratory system. Computer Methods and Programs in Biomedicine, 2009, 93, 20-31.	4.7	71
102	Comparison of envelope extraction algorithms for cardiac sound signal segmentation. Expert Systems With Applications, 2008, 34, 1056-1069.	7.6	187
103	Detection of valvular heart disorders using wavelet packet decomposition and support vector machine. Expert Systems With Applications, 2008, 35, 1679-1687.	7.6	68
104	A wearable cardiorespiratory sensor system for analyzing the sleep condition. Expert Systems With Applications, 2008, 35, 317-329.	7.6	27
105	A cardiac sound characteristic waveform method for in-home heart disorder monitoring with electric stethoscope. Expert Systems With Applications, 2006, 31, 286-298.	7.6	112
106	A novel wearable sensor device with conductive fabric and PVDF film for monitoring cardiorespiratory signals. Sensors and Actuators A: Physical, 2006, 128, 317-326.	4.1	202